PCCP

PAPER

View Article Online
View Journal | View Issue

Cite this: *Phys. Chem. Chem. Phys.*, 2015, **17**, 14613

Singlet and triplet excitons and charge polarons in cycloparaphenylenes: a density functional theory study†

Jin Liu,[a] Lyudmyla Adamska,*[b] Stephen K. Doorn[c] and Sergei Tretiak[bc]

The conformational structure and the electronic properties of various electronic excitations in cycloparaphenylenes (CPPs) are calculated using hybrid density functional theory (DFT). The results demonstrate that wavefunctions of singlet and triplet excitons as well as the positive and negative polarons remain fully delocalized in CPPs. In contrast, these excitations in larger CPP molecules become localized on several phenyl rings, which are locally planarized, while the undeformed ground state geometry is preserved on the rest of the hoop. As evidenced by the measurements of bond-length alternation and dihedral angles, localized regions show stronger hybridization between neighboring bonds and thus enhanced electronic communication. This effect is even more significant in the smaller hoops, where phenyl rings have strong quinoid character in the ground state. Thus, upon excitation, electron–phonon coupling leads to the self-trapping of the electronic wavefunction and release of energy from fractions of an eV up to two eVs, depending on the type of excitation and the size of the hoop. The impact of such localization on electronic and optical properties of CPPs is systematically investigated and compared with the available experimental measurements.

Received 26th March 2015,
Accepted 30th April 2015

DOI: 10.1039/c5cp01782c

www.rsc.org/pccp

1. Introduction

Cycloparaphenylenes ([*n*]CPPs) are a class of hoop-shaped conjugated molecules consisting of *n* repeating conjugated phenyl rings as depicted in Fig. 1 for [9]CPP. The first successful attempt of synthesis of CPPs can be traced back to 1993 targeting [6]–[10]CPPs.[1] However, the efficient high-yield synthesis of these molecules was pioneered by Jasti and co-workers in 2008.[2] Since then CPPs were studied by the groups of Itami,[3–5] Jasti,[2,6–11] Yamago[12–14] and many others.[9,15–19] Owing to the potential application as seeds for growing the single chirality metallic carbon nanotubes,[20] being efficient emitters with tunable wavelength,[13,21] and having a unique structure that inspired the synthesis of hoops with alternative building blocks[22] and cage-like structures,[23,24] CPPs very quickly acquired world-wide attention. Numerous studies were reported in selective syntheses,[5–7,12] measurement of optical properties[4,14,15] and theoretical modeling.[17–19,25–27] Here we refer the reader to the comprehensive recent review on the subject.[28] The "softness" of the CPP atomic structure, *i.e.* relatively low energetic cost of phenyl ring rotation, is expected to have a major effect on the dynamics of these molecules upon optical excitation and/or charging. The interplay between backbone strain,[7,10,29] steric interactions, competing aromatic and quinoid character of the carbon bonds (as evidenced by Raman spectroscopy[11,14,30]), and quantum confinement effects is complex since all the contributions from these competing interactions are of about the same order of magnitude and are finely tuned by changing the size of the hoop.

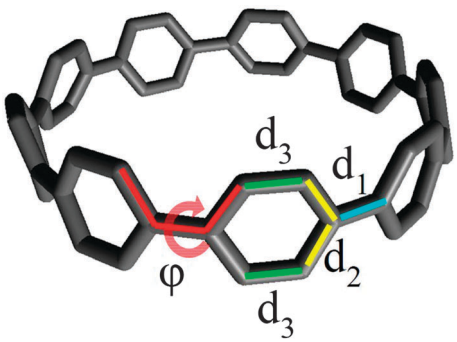

Fig. 1 Schematic representation of the dihedral angle φ and the nonequivalent bond lengths d_1–d_3 exemplified for [9]CPP. Hydrogen atoms are not shown.

[a] *Department of Chemical Engineering, University of Rochester, Rochester, New York 14627, USA*
[b] *Theoretical Division (T-1) and Center for Nonlinear Studies (CNLS), Los Alamos National Laboratory, Los Alamos, New Mexico 87545, USA. E-mail: mila@lanl.gov*
[c] *Center for Integrated Nanotechnologies (CINT), Los Alamos National Laboratory, Los Alamos, New Mexico 87545, USA*

† Electronic supplementary information (ESI) available. See DOI: 10.1039/c5cp01782c

For example, with increasing number of rings in [*n*]CPP, the backbone strain is slightly released, steric interactions increase, and quinoid-like character loses its strength to aromatic-like character. All these factors tend to increase the HOMO–LUMO gap with *n*; however, since the hoop size is increased, the box size for quantized excitations is increased as well, leading to the reduction of the respective band-gaps. One of the consequences of this complex interplay is a virtually constant optical absorption maximum of [*n*]CPPs at 340 nm regardless of the hoop size. However, this trend does not hold for optical properties of anionic and cationic species. Experimental and computational studies of photoabsorption in charged nanohoops were performed by Fujitsuka *et al.*[31] The authors observed that the energy of the lowest absorption state decreases with increasing hoop size. The fluorescence properties of CPPs are also dictated by many intricate interactions. As was shown in time-resolved optical experiments[13] and theoretical modeling based on excited state dynamics calculations and time-dependent DFT (TDDFT),[27] electron–phonon coupling leads to exciton self-trapping[32,33] on a time scale that is much shorter than the fluorescence lifetime, thus suggesting that all emission occurs from a spatially confined section of the hoop (4–5 phenyl rings).

Following an exhaustive set of experimental data, theoretical studies became pivotal in determining the structure–property relationship in [*n*]CPPs. The strain energies of CPPs were regarded as the main source of distinct properties of cyclic phenylenes compared to their linear counterparts.[29] Wong[17] in 2009 successfully reproduced the size-scaling of optoelectronic properties between linear and cyclic paraphenylenes. In 2010, Sundholm *et al.*[26] suggested that the excited state has a stronger electron delocalization around the carbon nanohoop than the ground state which is only true for small hoops as was recently shown.[27] In spite of the fascinating recent progress in theoretical work,[18,21,27] previous studies mostly focused on the ground states or low-energy singlet excited states, while spin states and polarons are rarely noted. Motivated by a good agreement between theory and numerous experiments[6,12,13,21] for singlet absorption and emission spectra, as well as recent experimental reports on triplet[15,16] and charged states of CPPs,[9,31] here we study computationally a set of significant electronic excitations defining optoelectronic functionalities in [*n*]CPP systems using DFT and TDDFT methodologies. In addition to the ground state (charge = 0, spin = 0) denoted as S_0, this set includes a manifold of singlet (charge = 0, spin = 0) and triplet (charge = 0, spin = 1) states as well as positive (charge = +1, spin = 1/2) and negative (charge = −1, spin = 1/2) polarons. The latter (cationic and anionic charged species) correspond to the presence of a hole or an electron on the molecule, respectively. The paper is organized as follows. Section 2 briefly discusses the computational methodology used. Section 3 overviews the obtained results for electronic and optical properties of these electronic excitations. Here we analyze the spatial extent of their wavefunctions, the impact of electron–phonon coupling and the respective various stabilization energies, as well as compare our modeling data to the available experiments. Finally, in Section 4, we conclude by summarizing our findings and observed trends.

2. Methods

All computations are performed using the Gaussian 09 suite[34] using the Coulomb attenuated B3LYP (CAM-B3LYP) hybrid functional[35] and the 6-31G* basis set. Ultrafine integration grid and tight geometry convergence criteria are employed in order to capture the small size-dependent changes in the atomic structure of [*n*]CPPs and reach the verified optimal structures of different electronic states. The effect of solvent is included in a framework of the conductor-like polarizable continuum model (CPCM) using the experimentally relevant dichloromethane solvent (ε_r = 9.02) as implemented in the Gaussian 09 package. As shown previously,[27] gas-phase calculations do not yield correct excited state geometries for singlet excitons and predict vanishing oscillator strength for fluorescence even in larger [*n*]CPPs in contrast to experimental observations.[2,13] It is important to stress that the popular GGA and hybrid (with the modest 20–25% fraction of orbital exchange) functionals such as PBE1[36] (also called PBE) and B3LYP[37] tend to smear the charges over the entire molecule and strongly delocalize the optical excitations.[27,38,39] Therefore, one has to use long-range corrected hybrid functionals in order to capture the correct physics.[38,39] Among the multiple kernels available,[35,40–43] we chose the simple CAM-B3LYP model where the fraction of orbital exchange varies between 20% and 65% on short and long distances, respectively, whereas the intermediate region is smoothly described using the standard error function with parameter 0.33. CAM-B3LYP provides a reasonable estimate for transition energies of singlet states in this class of molecules.[27,39] Any other conventional long-range corrected hybrid model will produce trends similar to CAM-B3LYP results.[27,44] Perhaps, for quantitative purposes, the use of the IP-tuned functionals,[45–47] would be preferable to describe the properties of individual CPP molecules. However, here we aim to capture the size-dependent trends in electronic and optical properties for the entire CPP series within the same functional framework.

The systems of interest are [*n*]CPPs with *n* ranging from 5 to 12 and 16. The optimal geometry of molecules in their singlet ground state is further referred to as S_0. Singlet and triplet excitons, and positive and negative polarons in the S_0 geometry are labeled as S_n, T_n, P_+ and P_-, respectively, where P_+ (P_-) denote a positively (negatively) charged molecule. All types of electronic excitations in their native optimal geometries are denoted with "*" (*e.g.*, S_{1^*}, T_{1^*}, P_{+^*} and P_{-^*}). Optimal geometries of S_0, T_1, P_+ and P_- states have been obtained using a standard self-consistent field (SCF) scheme, whereas the geometry of the S_1 state has been optimized using the TDDFT methodology. The latter approach is also used to calculate higher energy singlet and triplet states (S_n and T_n, $n > 1$).

Dihedral (torsion) angles and bond length alternation (BLA) parameters are used to characterize the geometric features of CPPs. Following previous studies,[14,48] BLA is a convenient single parameter reflecting the inhomogeneity in the distribution of

Table 1 Calculated ionization potential (IP), electron affinity (EA), fundamental energy gap (QEG), HOMO–LUMO gap (HL), exciton binding energy (E_{exc}) and stabilization energy (SE) of [*n*]CPPs

	IP (eV)	EA (eV)	QEG (eV)	HL (eV)	E_{exc} (eV)		SE (eV)			
n	P_{+*}–S_0	P_{-*}–S_0	P_{+*}, P_{-*}	S_0	P_+–P_-–S_1	P_{+*}–P_{-*}–S_{1*}	S_1–S_{1*}	T_1–T_{1*}	P_+–P_{+*}	P_-–P_{-*}
5	4.91	1.99	2.92	5.07	0.74	1.00	0.71	0.85	0.22	0.23
6	5.26	1.77	3.49	5.52	0.89	1.01	0.72	1.28	0.26	0.33
7	5.37	1.26	4.11	5.55	0.76	1.30	0.50	0.79	0.20	0.24
8	5.53	1.60	3.93	5.81	0.96	0.82	0.48	1.67	0.28	0.33
9	5.55	1.65	3.90	5.81	0.90	0.76	0.46	0.85	0.34	0.26
10	5.65	1.56	4.09	5.96	1.10	0.72	0.47	1.94	0.35	0.41
11	5.63	1.59	4.04	5.95	0.98	0.78	0.48	0.86	0.42	0.27
12	5.70	1.53	4.14	6.04	1.23	0.82	0.47	2.13	0.42	0.47
16	5.77	1.53	4.24	6.12	1.42	0.81	0.47	2.40	0.50	0.58

electrons along the polymer chain. The BLA is generally defined as a difference between single and double bond lengths along the cycle chain

$$\mathrm{BLA} = d_1 - d_2 \cdot \frac{2}{3} - d_3 \cdot \frac{1}{3}, \quad (1)$$

where d_{1-3} are depicted in Fig. 1. A smaller BLA value typically represents an enhancement of the electronic delocalization and a stronger π-conjugation. Reduction of the torsion angle ϕ (see Fig. 1) has a similar interpretation.

The electronic properties of CPPs are characterized in terms of ionization potential (IP), electron affinity (EA), HOMO–LUMO gap (HL) (in the ground state S_0) and electronic transition energies $\Omega(S_n)$ (or $\Omega(T_n)$). The IP/EA is defined as differences in total energies E between the charged systems and the neutral ground state as follows

$$\mathrm{IP} = E(P_{+*}) - E(S_0), \quad (2)$$

$$\mathrm{EA} = E(S_0) - E(P_{-*}). \quad (3)$$

The difference between IPs and EAs defines the quasiparticle energy gap (QEG) or the fundamental gap[49]

$$\mathrm{QEG} = \mathrm{IP} - \mathrm{EA}. \quad (4)$$

The stabilization energy (SE) of an electronic excitation is defined as a change in the total energy during geometry optimization from the ground state to the 'native' geometry. For example, the triplet SE is computed as

$$\mathrm{SE}(T_1 \rightarrow T_{1*}) = E(T_1) - E(T_{1*}). \quad (5)$$

The singlet exciton binding energy is evaluated as[17]

$$E_{exc} = \mathrm{QEG} - \Omega(S_{1*}), \quad (6)$$

where $\Omega(S_{1*})$ is the energy of the lowest singlet state S_{1*} in its optimal geometry (emission point). The vibronic ($\Delta\Omega$) and vibrational ($\delta\Omega$) Stokes shifts are defined as the difference between the corresponding vertical transition energies as

$$\Delta\Omega = \Omega(S_{2/3}) - \Omega(S_{1*}), \quad (7)$$

$$\delta\Omega = \Omega(S_1) - \Omega(S_{1*}). \quad (8)$$

Here the former quantity constitutes the difference between optically active degenerate S_2/S_3 states and the emission state S_{1*}, which is directly relevant to the red shift between experimental UV-vis absorption and fluorescence peak maxima. In contrast, $\delta\Omega$ reflects the vibrational relaxation of the lowest singlet state S_1 and may be probed by nonlinear and time-resolved spectroscopy.[50]

Table 2 Vertical transition energies (Ω) and oscillator strengths of significant singlet state absorption (S_1–S_3). The vibronic ($\Delta\Omega$) and vibrational ($\delta\Omega$) Stokes shifts are defined in eqn (7) and (8)

	Absorption						Fluorescence		Stokes shifts (eV)	
	S_1		S_2		S_3		S_{1*}			
n	Ω (eV)	*f*	Ω (eV)	*f*	Ω (eV)	*f*	Ω (eV)	*f*	$\Delta\Omega$	$\delta\Omega$
5	2.63	0.00	4.05	0.27	4.10	0.63	1.27	0.0	2.81	1.36
6	3.19	0.00	4.16	1.17	4.16	1.17	1.83	0.0	2.33	1.36
7	3.31	0.03	4.05	1.55	4.13	1.56	2.20	0.002	1.89	1.11
8	3.58	0.00	4.13	1.88	4.13	1.88	2.62/2.56	0.0/0.44	1.57	1.02
9	3.60	0.07	4.04	2.18	4.12	2.22	2.67	0.89	1.41	0.93
10	3.75	0.00	4.11	2.57	4.11	2.57	2.74	1.20	1.37	1.01
11	3.74	0.10	4.04	2.83	4.11	2.90	2.79	1.45	1.29	0.95
12	3.83	0.00	4.10	3.26	4.10	3.26	2.82	1.67	1.28	1.01
16	3.90	0.00	4.07	4.64	4.07	4.64	2.93	2.31	1.14	0.97

The calculated electronic and optical quantities for unrelaxed (T_1, P_+, P_-, S_n) and relaxed (T_{1*}, P_{+*}, P_{-*}, S_{1*}) excitations are compiled in Tables 1–3. Table 1 summarizes the size-dependent trends of such quantities as stabilization energy, electron affinity and ionization potential, quasi-particle energy gap, HOMO–LUMO gap, and exciton binding energy. Table 2 is devoted to the optical properties of singlet excitations. Absorption states S_n are computed by running the TDDFT simulation for CPPs in their S_0 geometries. The fluorescence state S_{1*} (the lowest singlet excited state relevant *via* Kasha's rule[51]) geometry is optimized using the TDDFT framework. Table 3 summarizes the data on the triplet state manifold. Triplet excited states T_n are calculated using triplet TDDFT simulations using S_0 geometry, only excitation energies $\Omega(T_n)$ are shown since these transitions are optically forbidden. The triplet state absorption (*i.e.*, absorption from the lowest metastable state T_1 to T_n) is evaluated by calculating the respective energy differences and transition dipoles/oscillator strengths. We have identified the three lowest triplet absorption bands. Finally, phosphorescence energy is evaluated from the difference in total energies of the molecule in the lowest triplet and singlet states in T_{1*} geometry. Table 4 summarizes the available experimental data for comparison.

Additionally, natural orbitals (NOs) reflecting the spatial delocalization of the unpaired electron wavefunctions are

Table 3 Vertical transition energies (Ω) of significant triplet excited states (T_1–T_5). Transition energies and oscillator strengths for the lowest triplet absorption bands and phosphorescence spectra

	Triplet excited states					Triplet absorption						Triplet phosphorescence
n	$\Omega(T_1)$ (eV)	$\Omega(T_2)$ (eV)	$\Omega(T_3)$ (eV)	$\Omega(T_4)$ (eV)	$\Omega(T_5)$ (eV)	Ω (eV)	f	Ω (eV)	f	Ω (eV)	f	Ω (eV)
5	1.51	2.35	2.35	3.37	3.44	2.09	0.003	3.07	0.91	4.49	0.01	1.50
6	2.01	2.48	2.48	3.29	3.29	2.02	0.015	2.85	0.77	4.55	0.15	1.91
7	2.09	2.44	2.52	3.17	3.17	2.10	0.007	2.80	0.75	4.49	0.05	2.09
8	2.33	2.56	2.56	3.09	3.09	1.86	0.008	2.76	0.67	4.01	0.13	2.23
9	2.32	2.52	2.59	2.99	3.02	1.93	0.003	2.76	0.64	3.87	0.11	2.26
10	2.46	2.60	2.60	2.96	2.96	1.81	0.005	2.77	0.63	3.68	0.13	2.38
11	2.44	2.57	2.62	2.88	2.94	1.87	0.002	2.77	0.54	3.59	0.10	2.39
12	2.52	2.62	2.62	2.88	2.88	1.79	0.004	2.78	0.63	3.47	0.14	2.48
16	2.59	2.64	2.64	2.80	2.80	1.78	0.002	2.78	0.67	3.33	0.08	2.59

Table 4 Available experimental data on optical excitations in CPPs, excitation energies (Ω) and fluorescence quantum yields (Φ)

	Singlet absorption	Singlet fluorescence		Two-photon absorption	Triplet absorption	Triplet phosphorescence
n	Ω (eV)	Ω (eV)	Φ	Ω (eV)	Ω (eV)	Ω (eV)
5	3.70[i,j]	—	0.0[j]	—	—	—
6	3.65[e]	—	0.0[e]	—	—	—
7	3.65[h]	2.11[h]	0.01[e,h]	—	—	—
8	3.65[d], 3.67[c]	2.33[c,d]	0.08[c], 0.1[e]	—	—	1.85[j]
9	3.64[d], 3.65[a,c,f], 3.66[b]	2.48[d,f], 2.51[a,b,c]	0.3[c], 0.38[e], 0.73[b]	3.06[f]	3.18[k]	1.96[j]
10	3.64[d], 3.65[c]	2.62[d], 2.64[c]	0.46[c], 0.65[e]	—	—	2.03[j]
11	3.65[d], 3.66[c]	2.70[c,d]	0.52[c], 0.73[e]	—	—	2.07[j]
12	3.65[a], 3.66[d,f], 3.67[b,c]	2.75[a,b,c,d,f], 2.67[g]	0.66[c], 0.81[e], 0.89[b]	3.20[f]	1.82[k]	2.10[j]
16	3.67[d], 3.66[b,f]	2.83[b,f]	0.88[b]	3.26[f]	—	—

[a] Ref. 2. [b] Ref. 21. [c] Ref. 13. [d] Ref. 12. [e] Ref. 6. [f] Ref. 4. [g] Ref. 20. [h] Ref. 8. [i] Ref. 10. [j] Ref. 16. [k] Ref. 15.

analyzed for triplet and charged states. To perform a similar evaluation for singlet excitonic states, we further use orbital plots of transition densities (or density plots, *i.e.*, the diagonal of the transition density matrix for a state of interest projected onto the atomic orbital basis). Finally, the structure of higher energy excited states is characterized using the density of excited states (DOES) computed for singlet and triplet electronic spectra. The positions of singlet S_n and triplet T_n transitions are compiled in histograms for a compact representation.

3. Results and discussion

3.1. Geometries of excited states

The ground state geometries of [n]CPPs have been discussed in several theoretical reports.[11,17,21,30] It is shown that the ground state geometries are a consequence of a complex interplay between steric interactions, π-conjugation and backbone strain. Even-numbered [n]CPPs can adopt a high symmetry configuration with dihedral angles alternating as $\pm\varphi$, whereas odd-numbered hoops connect the n-th ring to its neighbors by a dihedral angle of $\varphi/2$ while preserving the $\pm\varphi$ pattern on the rest of the $n-1$ phenyl rings. The portion of the hoop with $\varphi/2$ dihedral angles is further called a "*natural defect*" of the odd-numbered CPPs, reflecting the presence of a frustrated structure. Raman spectroscopy[14,30] on [n]CPPs (n = 6, 8–12) unveiled that the bands resulting from C=C/C–C stretches experience a significant shift with increasing n, indicating that quinoidal character is more profound in small CPPs, thus explaining why smaller hoops have smaller dihedral angles and smaller band gaps.[14,52] The geometries of CPPs in the ground state and all considered electronic excitations are shown in Fig. S1 in the ESI.† The quantitative description of size-dependent structural changes in CPPs can be obtained by inspecting the dihedral angles in the ground state (black bars) and excited states (color-coded bars) in Fig. 2.

Generally, we observe the highly symmetric structure in the ground state and a local planarization developing over several phenyl rings in all excited states in large molecules, which gradually disappears with reduction of the hoop size. In the case of singlet relaxed excitons S_{1^*}, [8]CPP is energetically quasi-degenerate – its lowest energy state (not shown in Fig. 2) is highly symmetric with dihedral angles of $\pm 13^\circ$, and the deformed geometry conformer (shown in Fig. 2(a)) is only 27 meV higher in energy. Thus at room temperature both structures can co-exist. [n]CPPs with $n < 8$ have uniform geometries reflecting fully delocalized singlet excitations. In the case of the triplet state T_{1^*}, all hoops with $n > 5$ have local deformations (Fig. 2(b)). In addition to the local chain planarization, the hoop is becoming distorted from a circular to an egg-shaped form during triplet state relaxation, see Fig. S1 in the ESI.† Similar to triplets, positively and negatively charged CPPs (P_{+^*} and P_{-^*} states) also show local deformations in hoops with $n > 6$ (Fig. 2(c) and (d)). Overall, geometry distortions in the case of triplets and polarons are significantly stronger than those in singlet excitations (compare columns in Fig. 2). Similar to our results, an elliptical distortion of the CPPs due to multiple charging has been previously reported in ref. 9.

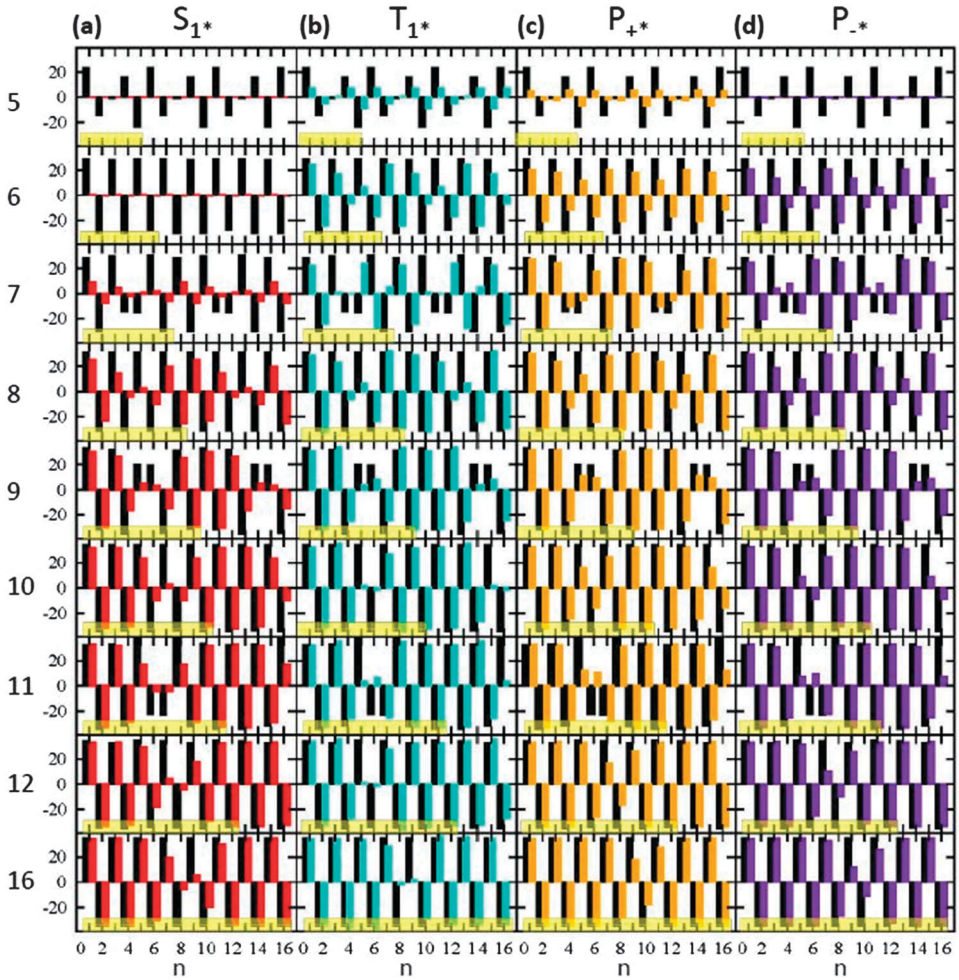

Fig. 2 Dihedral angles (degrees) in [*n*]CPPs for different types of excitations: singlet excitons S_{1*} ((a), red bars), triplet excitons T_{1*} ((b), cyan bars), positively charged polarons P_{+*} ((c), orange bars) and negatively charged polarons P_{-*} ((d), violet bars). Dihedral angles of [*n*]CPPs in the ground state geometry S_0 are shown in black bars on each subplot. The length of the hoop is marked by the yellow semitransparent rectangle, shorter hoops are periodically replicated.

In addition to the local planarization of phenyl rings, the structural changes in CPPs upon excitation are also accompanied by changes in bond lengths. These changes constitute the major contribution to the total energy – the influence of torsional changes in phenyl rings on the total energy of the system is only moderately significant.[21,53] In order to examine the changes in carbon–carbon bond lengths, we plot the bond length alternation parameter (BLA, see eqn (1) in Methods section) in the localized and undeformed regions of excited CPPs in Fig. 3. A large value of BLA signifies the quinoid character of the carbon backbone, *i.e.*, alternating single/double bonds, and a small value of BLA reflects an increase of aromaticity in the carbon backbone and the electron delocalization on neighboring bonds. The behavior of the BLA in the undeformed regions of CPPs (Fig. 3(a)) approaches the BLA of the ground state S_0 in larger hoops. The BLA in localized regions (Fig. 3(b)) shows a flat behavior for those hoops that are large enough for excitations to localize. Generally, excitations localize on about 5 phenyl rings, therefore, the BLA is size-dependent in localized regions of small hoops. The red open circle in Fig. 3(b) refers to the uniformly deformed [8]CPP. It is clear from the graph that this structure continues the size-dependent trend of smaller hoops.

3.2. Electronic properties

3.2.1. Stabilization energy of electronic excitations. Concomitant to geometrical changes, the stabilization energy summarized in Table 1 is a convenient descriptor showing the overall gain in total energy due to structural deformations (eqn (5) in Methods section). The stabilization energy of triplets is the largest among the four species considered, up to 2 eV, owing to very large structural changes[38,39] including even distortions to an egg-shape. This quantity progressively increases from small to large hoops. Notably, odd-ring hoops with a natural defect have significantly smaller triplet SEs compared to their similar-sized even-ring counterparts, indicating smaller relaxation in already distorted structures, where the natural defect serves as an initial localization spot. Similar trends persist for polarons, albeit the polaron SE is much smaller compared to the triplet one, being a fraction of an eV. Positive and negative polarons have similar SE, which reflects an approximate symmetry of valence and

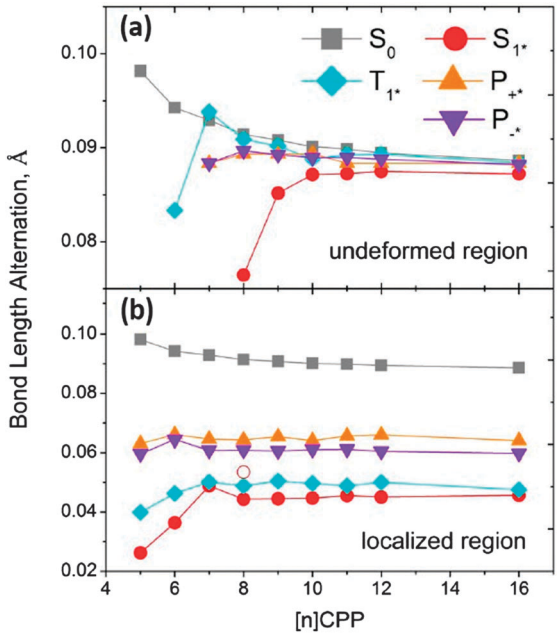

Fig. 3 Bond length alternation (BLA, see eqn (1)) in undeformed (a) and localized (b) regions for singlets S_{1*}, triplets T_{1*}, and positive P_{+*} and negative P_{-*} polarons. The BLA in the ground state geometry S_0 is shown on both plots for comparison.

conduction bands of CPPs in the absence of electron donating/withdrawing groups. Notably, the polaron SEs alternate between odd- and even-numbered [*n*]CPPs (*i.e.*, generally, SE (P_+) < SE (P_-) and SE (P_+) > SE (P_-) for even- and odd-numbered systems, respectively). This is attributed to different atomistic localizations of the additional charge density – the positive charge is mostly localized on the backbone carbons, whereas the negative charge is hosted by peripheral carbons bonded to hydrogens. Subsequently, P_+ is more sensitive to the backbone conformation compared to P_-. Furthermore, we recall that the SE of charged states gains from both geometry relaxation and polarization effects, the latter being larger for a smaller polaron size. In contrast to the spin and charged states, the trend in the stabilization energy for singlets is opposite to the molecular size – the singlet exciton SE is about 0.5 eV being nearly constant in the hoops large enough to provide the exciton localization. Conversely, in the highly strained small CPPs, the SE is increased to 0.7 eV (see Table 1), indicating possible gains from delocalization of through-space interactions. The stabilization energy of the singlet exciton is crucial for fluorescence dynamics, determining the blueshift of fluorescence emission.

3.2.2. Triplet and charged states. Natural orbitals (NOs) calculated for unpaired electrons or orbital visualization of spin density are two common descriptors defining spatial delocalization/localization of spin state wave functions (*e.g.*, triplets and polarons). Fig. 4(a) and (b) depicts the NOs of both unpaired electrons in unrelaxed T_1 and geometry optimized T_{1*} states, respectively. The reader readily observes that all relaxed T_{1*} are spatially localized in all hoops larger than [5]CPP concomitant to geometry changes described above. In contrast to singlet states,[27] localization of unrelaxed T_1 excitations is also (and only)

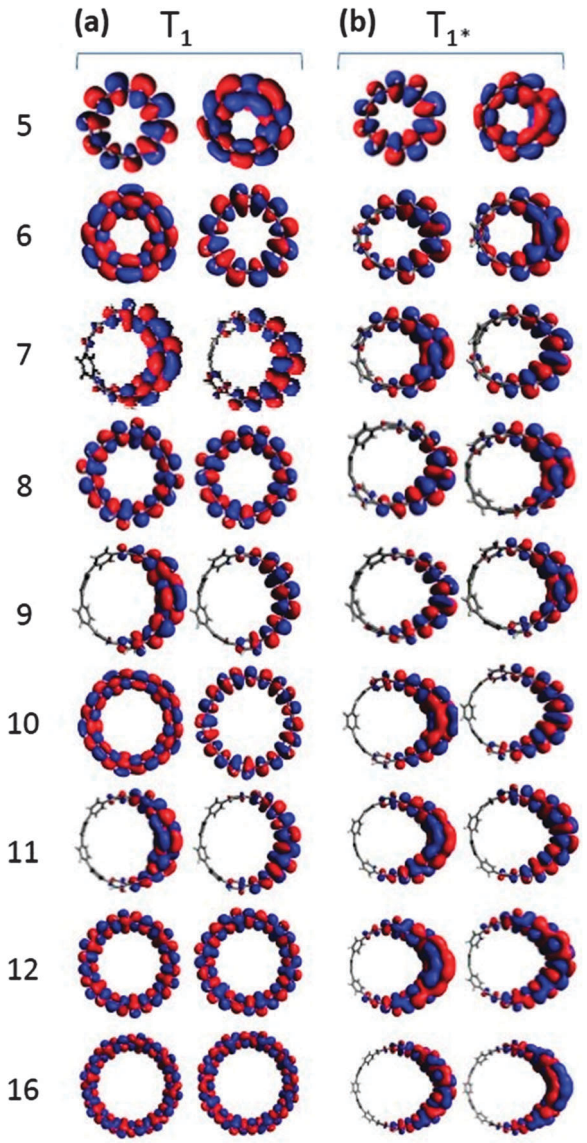

Fig. 4 Natural orbitals (NOs) of unpaired electrons in the lowest triplet state. NOs in unrelaxed systems (T_1) are localized (delocalized) in odd- (even-) numbered [*n*]CPPs. In contrast, relaxed triplet states T_{1*} are localized in all molecules with $n > 5$.

observed in odd-numbered CPPs. Both unpaired electrons are attracted to the planarized portion of the hoop or the natural defect in odd-numbered CPPs. The unrelaxed T_1 states in even-numbered CPPs stay delocalized. As follows from the dihedral angle analysis (Fig. 2), the localization region of triplets is very small. The localization/delocalization properties of NOs correlate well with the behavior of the respective spin density, see Fig. S2 and S3 in the ESI.†

Ionization potential (IP) and electron affinity (EA) evaluated using eqn (2) and (3) in the Methods section, respectively, provide important electronic characteristics relevant to the molecular response to charging and functionality of the system in the device environment. Summarized in Table 1, IPs and EAs calculated for the CPP family are expected to reflect well the trends across the molecular family, while the absolute values of

numbers are likely to be systematically shifted from the respective experimentally measured quantities.[54] Noticeably, calculated IPs and EAs vary up to 1 eV as a function of CPP hoop size, see Table 1 – the IP increases from 4.9 eV to 5.8 eV, whereas the EA decreases from 2 to 1.5 eV as n increases from 5 to 16. IPs and EAs change with different slopes as a function of n in odd- and even-numbered hoops. Here our calculated IP and EA values differ from the respective numbers reported previously,[17] due to geometry optimization of charged species and incorporation of solvent effects in this work, whereas ref. 17 was based on unrelaxed gas phase calculations. Our calculations show that the fundamental gap (QEG) calculated using eqn (4) in the Methods section is 3 eV in [5]CPP and 3.5 eV in [6]CPP. These smallest hoops have both polarons delocalized. In hoops larger than 7 phenyl units (localized polarons) QEG jumps to 4 eV and then increases slowly to 4.2 eV in [16]CPP. For comparison, Table 1 lists HOMO–LUMO gaps as well. The QEG and HOMO–LUMO gaps have qualitatively similar size-dependent shifts (up to $\sim$2 eV constant shift) but the latter (calculated in the ground state) do not show abrupt changes due to delocalization/localization transition. Our HOMO–LUMO gaps agree quite well with previously reported simulations[18] performed using the B3LYP hybrid functional and chloroform solvent up to a constant of $\sim$2 eV blueshift resulting from the use of the range-corrected functional. As expected, the HOMO–LUMO gaps are weakly sensitive to the dielectric environment.

Fig. 5 depicts the natural orbitals of charged states in the unrelaxed P_+/P_- and geometry optimized P_{+*}/P_{-*} structures. Similar to triplets, charged states generally spatially localize on a few phenyl rings as well. A "natural" defect in dihedral angles of odd-numbered [n]CPPs is sufficient to localize those excitations even in the ground state geometry (see Fig. 5(a and c)). One readily observes that NOs of P_+/P_- in even-numbered [n]CPPs are delocalized regardless of the hoop size, but in P_{+*}/P_{-*} systems the charged states always localize for all hoops with $n > 6$. Both electron (P_-/P_{-*}) and hole (P_+/P_{+*}) polarons, if localized, are pinned to the planarized section of the hoop.

3.2.3. Singlet excited states. The exciton binding energy provides a quantitative measure of Coulomb electron–hole interactions. This quantity can be evaluated as a difference between the fundamental gap and the optical gap (eqn (6) in Methods section). The result may depend on the DFT model used, and, therefore, we will follow the trends across the CPP series. The calculated exciton binding energy is $\sim$0.8 eV, being about constant for localized singlet excitons. The small molecules, where excitons remain delocalized, have a larger binding energy of $\sim$1 eV. Such an increase is attributed to an effect of quantum confinement facilitating stronger electron–hole interactions compared to an unconfined exciton. In order to stress the importance of geometry optimization for systems with "soft" torsional degrees of freedom, like CPPs, we have computed the exciton binding energy without vibrational relaxation (see the P_+–P_-–S_1 column in Table 1). The exciton binding energy increases with the size of [n]CPP if unrelaxed values $E(P_+)/E(P_-)$ are used in the calculation of IP/EA, and $\Omega(S_1)$ is used for the optical gap. The size-dependent trend of *unrelaxed* exciton binding energy *contradicts* the intuitive quantum confinement arguments.

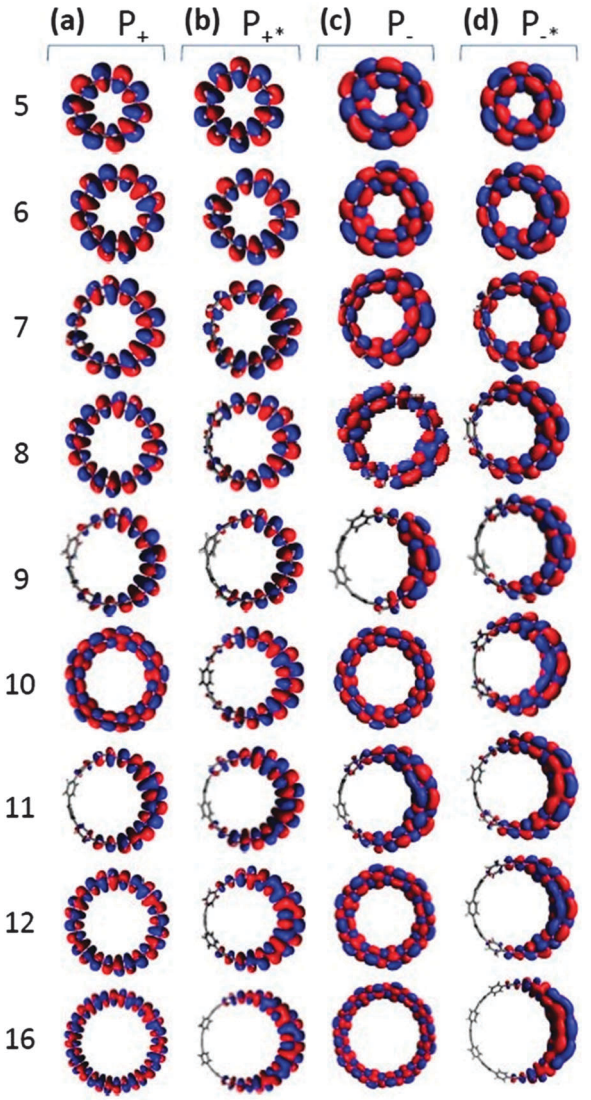

Fig. 5 Natural orbitals (NOs) of unpaired elections in charged states. NOs of unrelaxed charged systems P_+/P_- are localized only in odd-numbered [n]CPPs. In contrast, all relaxed polarons (P_{+*}/P_{-*}) are localized in hoops with $n > 6$.

In order to visualize the localized/delocalized patterns of singlet excitons, in Fig. 6 we plot the orbital projection of transition density (see Methods) for singlet states shown in Table 2. The vector (not shown) drawn from blue to red regions of transition density roughly corresponds to the direction of the electronic transition dipole moment. The S_1 state is optically forbidden due to symmetry, and the transition density of this state is uniformly smeared around the hoop (Fig. 6(a)). In contrast, S_2 and S_3 states are optically allowed and degenerate/quasi-degenerate in even/odd numbered [n]CPPs, see Table 2. It is evident from Fig. 6(b and c) that these states have large transition dipole moments, which increase with the hoop size. This correlates with the calculated size-dependent trends of the oscillator strengths – larger hoops are better absorbers. All singlet excitonic

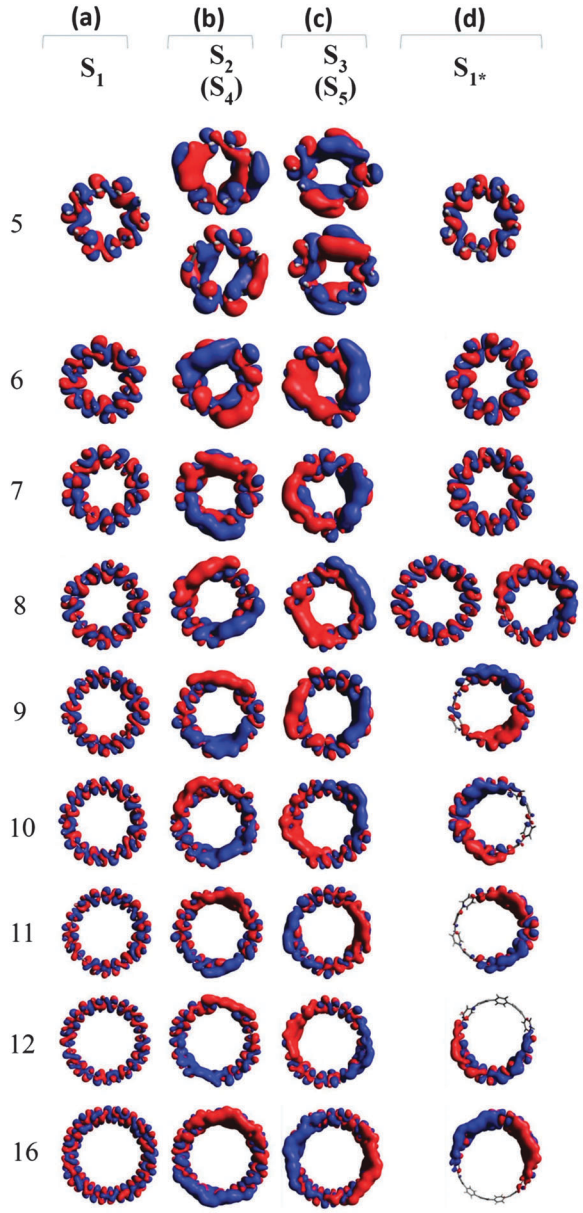

Fig. 6 Orbital plots of transition density in [*n*]CPPs for absorption states (S_1, S_2, and S_3) and the emission state S_{1*}. [5]CPP has 4 optically accessible states (S_2–S_5), while larger hoops have only 2 (S_2 and S_3). The first excited state S_1 is optically forbidden as evident from the symmetry of their transition dipoles.

states at S_0 geometry are fully delocalized. Here we do not observe even/odd alternation of delocalization/localization behavior that is inherent to triplets and charged states. However, the emission states at S_{1*} geometry in large hoops have planarized portions of the rings (Fig. 2(a)), where the self-trapped excitonic wavefunction resides.[27] Fig. 6(d) depicts the corresponding orbital distributions of transition density in emission states – they are spatially delocalized (localized) in hoops with $n < 8$ ($n > 8$), whereas [8]CPP has quasi-degenerate excited state structures, as shown in the left and right plots in Fig. 6(d).

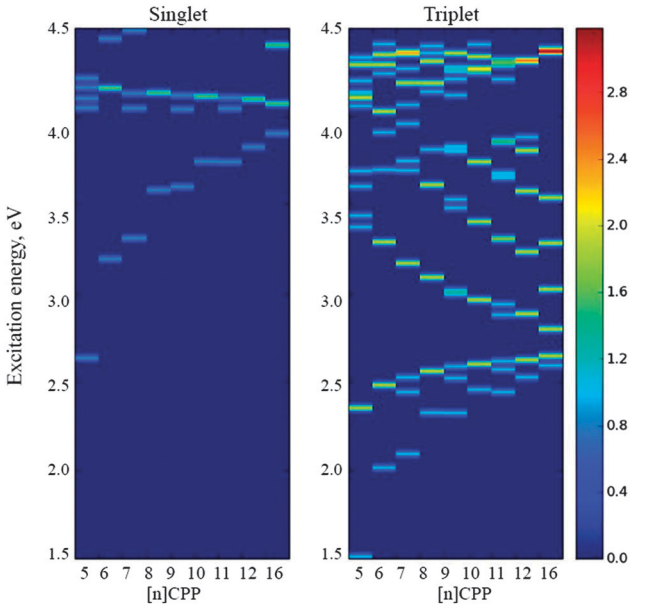

Fig. 7 Density of excited states (DOES) for singlet (a) and triplet (b) excited states. Light blue, green and red colors correspond to singly, doubly, and multiply (>2) degenerate levels, respectively. The levels are broadened with k_BT = 25 meV full width at half maximum.

3.3. Optical properties

3.3.1. Singlet state absorption and fluorescence. The computed absorption and fluorescence data are compiled in Table 2. The calculated vertical transition energies of the S_2/S_3 states exhibit a constant blue-shift of 0.48 eV compared to experimental absorption maxima in [*n*]CPPs summarized in Table 4,[2,13] being a typical feature of range-corrected functionals such as CAM-B3LYP. It is found that the vertical excitation energy from the ground state to the lowest S_1 state increases with the size of [*n*]CPPs, from 2.63 to 3.90 eV. Ref. 4 probed this state using two-photon absorption. Accounting for the constant blue-shift, our computational results regarding the S_1 transition energy agree well with experimental data in Table 4.

The size-dependent trends in optical absorption in cycloparaphenylenes are quantitatively different compared to linear conjugated oligomers or polymers, where typically the lowest band-gap state S_1 dominates optical absorption and its transition energy red-shifts with an increase of the oligomer length.[55] In CPPs, the S_1 state is optically forbidden across the entire family (barring small deviations due to strain and the presence of the natural defect), and its transition energy blue-shifts with an increase of the molecular size[27] (see Fig. 7(a)). Optically allowed S_2 and S_3 states (see Table 2) are responsible for the nearly constant-energy absorption peak, see more details in ref. 17, 18, 21 and 25. This agrees with multiple experiments, see Table 4. The relative positions of the absorption peaks as a function of CPP hoop size *n* are visualized in Fig. 7(a). S_2 and S_3 states are degenerate in even-numbered CPPs and quasi-degenerate in odd-numbered ones. [5]CPP is the exception – it is so strained that the oscillator strength from S_2 and S_3 transfers to S_4 and S_5 (which are optically forbidden in larger hoops). Here states S_2–S_5

are near-degenerate and have non-zero oscillator strength, S_5 mirrors S_2 and S_4 mirrors S_3 (see Fig. 7(a)).

Efficient fluorescence from large CPPs is attributed to the violation of the Condon approximation[56] as shown in ref. 27. Here, localization of the emissive state in distorted S_{1^*} geometries leads to the appearance of a significant transition dipole moment/oscillator strength. Subsequently, the fluorescence occurs from the lowest singlet state complying with Kasha's rule.[51] The calculated vertical transition energies for emission (Table 2) are in good agreement with experimental results (Table 4) and size-dependent trends for oscillator strength correlate well with the experimental fluorescence quantum yields Φ[6,13] – small hoops do not emit light, [8]CPP has $\Phi \sim 10\%$, Φ jumps to about 50% in [9]CPP and monotonically increases in larger hoops, see Table 4 for more details. Notably, the Stokes shift in all CPPs has both electronic and vibrational origin (Table 2), in contrast to the conjugated oligomer case where typically only vibrational relaxation contributes to the Stokes shifts.

3.3.2. Triplet state manifold, triplet absorption and phosphorescence. The calculated triplet density of excited states (DOES, see Methods) is shown in Fig. 7(b). The three lowest triplet states T_1–T_3 show size-dependent trends similar to S_1, *i.e.* blue-shift with an increase of the hoop size. T_4–T_6 behave in an opposite way. The transition energy values for the lowest five triplet states T_1–T_5 are summarized in Table 3. The triplet absorption is calculated using the approach described in the Methods section. The three lowest absorption bands are listed in Table 3 in the "Triplet absorption" column, where each band consists of two degenerate or nearly degenerate levels. Average energies and oscillator strengths are shown for a compact view. Overall, the second absorption band has a much larger, virtually size-independent oscillator strength compared to that of the other two. Vertical transition energies for triplet absorption show weak red-shifts with an increase of the molecular size.

Owing to weak spin–orbit coupling, intersystem crossing in CPPs is inefficient. Consequently, the population of triplet states is stimulated in experiments by adding a triggering agent, such as triplet oxygen.[15,16] The experimental measurement of triplet absorption of [9]- and [12]-CPPs in the presence of triplet oxygen was recently reported.[15] While triplet absorption maxima of 390 nm (3.18 eV) and 680 nm (1.82 eV) were assigned to [9]- and [12]-CPPs, respectively, the experimentally measured triplet absorption profiles in ref. 15 are very broad with three wide peaks of about the same wavelength (deviation <50 nm) but with slightly different intensities present in both molecules. The absorption peaks in [9]CPP appear slightly blue-shifted compared to [12]CPP, which qualitatively agrees with our computed trends.

The calculated and experimental data on phosphorescence are shown in Tables 3 and 4, respectively. Recent experimental work[16] suggests $\sim$100 microsecond triplet emission decay in [8]–[12]CPPs. In good agreement with computational results, the phosphorescence appears blue-shifted with an increase in the hoop size of [*n*]CPPs, albeit with smaller blue-shifts compared to the respective trends in fluorescence.

4. Conclusions

In summary, we report a detailed computational investigation of the structural, electronic, and optical properties of cycloparaphenylenes ([*n*]CPPs, n = 5–12, 16) using DFT and TDDFT techniques by characterizing essential electronic excitations comprising singlet (S_n) and triplet (T_n) state manifolds relevant to optical absorption, fluorescence (S_{1^*}) and phosphorescence (T_{1^*}) states, and positively (cations, P_+/P_{+^*}) and negatively (anions, P_-/P_{-^*}) charged systems (polarons). Our detailed analysis includes side-dependent trends in absorption/emission, relaxation/stabilization energies, ionization potential and electron affinity, which are compared when possible to experimental data. The overall calculated spectroscopic observables quantitatively agree with multiple experiments and reproduce important size-dependent trends. The main observation of this work is spatial localization of all excitations – singlet and triplet excitons and polarons. The structural changes between the ground state and excited states (S_{1^*}, T_{1^*}, P_{+^*}, P_{-^*}) are characterized in terms of dihedral angles, bond length alternation, and stabilization energies. Along with analysis of the spatial distribution of electronic wavefunctions (as reflected by natural orbitals and transition densities), this suggests that excitations and charges will self-trap on locally planarized sections of the hoop starting from some critical size. Notably, triplets and charged states are significantly more localized than excitons. In particular, such an exciton localization results in a violation of the Condon approximation, making cycloparaphenylenes to be efficient fluorophores.

Our current study provides valuable insights into the conceptual connection between conformational structures and electronic/optical properties in strained circular conjugated organic molecules. We believe that an understanding of the structural, electronic, and optical properties of CPPs as a function of the hoop size achieved in this work will motivate further experimental studies and stimulate the future design of CPP-based optoelectronic devices.

Acknowledgements

This work was supported by the U.S. Department of Energy and Los Alamos LDRD funds. Los Alamos National Laboratory is operated by the Los Alamos National Security, LLC, for the National Nuclear Security Administration of the U.S. Department of Energy under contract DE-AC5206NA25396. We acknowledge support from the Center for Integrated Nanotechnologies (CINT) and the Center for Nonlinear Studies (CNLS) at LANL.

References

1 R. Friederich, M. Nieger and F. Vögtle, *Chem. Ber.*, 1993, **126**, 1723.
2 R. Jasti, J. Bhattacharjee, J. B. Neaton and C. R. Bertozzi, *J. Am. Chem. Soc.*, 2008, **130**, 17646.
3 H. Omachi, Y. Segawa and K. Itami, *Acc. Chem. Res.*, 2012, **45**, 1378.

4 T. Nishihara, Y. Segawa, K. Itami and Y. Kanemitsu, *J. Phys. Chem. Lett.*, 2012, **3**, 3125.
5 Y. Ishii, Y. Nakanishi, H. Omachi, S. Matsuura, K. Matsui, H. Shinohara, Y. Segawa and K. Itami, *Chem. Sci.*, 2012, **3**, 2340.
6 E. R. Darzi, T. J. Sisto and R. Jasti, *J. Org. Chem.*, 2012, **77**, 6624.
7 T. J. Sisto, M. R. Golder, E. S. Hirst and R. Jasti, *J. Am. Chem. Soc.*, 2011, **133**, 15800.
8 P. Li, T. J. Sisto, E. R. Darzi and R. Jasti, *Org. Lett.*, 2013, **16**, 182.
9 A. V. Zabula, A. S. Filatov, J. Xia, R. Jasti and M. A. Petrukhina, *Angew. Chem.*, 2013, **125**, 5137.
10 P. J. Evans, E. R. Darzi and R. Jasti, *Nat. Chem.*, 2014, **6**, 404.
11 H. Chen, M. R. Golder, F. Wang, R. Jasti and A. K. Swan, *Carbon*, 2014, **67**, 203.
12 T. Iwamoto, Y. Watanabe, Y. Sakamoto, T. Suzuki and S. Yamago, *J. Am. Chem. Soc.*, 2011, **133**, 8354.
13 M. Fujitsuka, D. W. Cho, T. Iwamoto, S. Yamago and T. Majima, *Phys. Chem. Chem. Phys.*, 2012, **14**, 14585.
14 M. Fujitsuka, T. Iwamoto, E. Kayahara, S. Yamago and T. Majima, *ChemPhysChem*, 2013, **14**, 1570.
15 D. A. Hines, E. R. Darzi, R. Jasti and P. V. Kamat, *J. Phys. Chem. A*, 2014, **118**, 1595.
16 M. Fujitsuka, C. Lu, T. Iwamoto, E. Kayahara, S. Yamago and T. Majima, *J. Phys. Chem. A*, 2014, **118**, 4527.
17 B. M. Wong, *J. Phys. Chem. C*, 2009, **113**, 21921.
18 C. Camacho, T. A. Niehaus, K. Itami and S. Irle, *Chem. Sci.*, 2013, **4**, 187.
19 B. M. Wong and J. W. Lee, *J. Phys. Chem. Lett.*, 2011, **2**, 2702.
20 H. Omachi, T. Nakayama, E. Takahashi, Y. Segawa and K. Itami, *Nat. Chem.*, 2013, **5**, 572.
21 Y. Segawa, A. Fukazawa, S. Matsuura, H. Omachi, S. Yamaguchi, S. Irle and K. Itami, *Org. Biomol. Chem.*, 2012, **10**, 5979.
22 H. Shimizu, J. D. Cojal González, M. Hasegawa, T. Nishinaga, T. Haque, M. Takase, H. Otani, J. P. Rabe and M. Iyoda, *J. Am. Chem. Soc.*, 2015, **137**, 3877.
23 J. D. Evans, C. J. Sumby and C. J. Doonan, *Chem. Lett.*, 2015, **44**, 582.
24 E. Kayahara, *et al.*, *Nat. Commun.*, 2013, **4**, 2694.
25 V. S. Reddy, C. Camacho, J. L. Xia, R. Jasti and S. Irle, *J. Chem. Theory Comput.*, 2014, **10**, 4025.
26 D. Sundholm, S. Taubert and F. Pichierri, *Phys. Chem. Chem. Phys.*, 2010, **12**, 2751.
27 L. Adamska, I. Nayyar, H. Chen, A. K. Swan, N. Oldani, S. Fernandez-Alberti, M. R. Golder, R. Jasti, S. K. Doorn and S. Tretiak, *Nano Lett.*, 2014, **14**, 6539.
28 S. E. Lewis, *Chem. Soc. Rev.*, 2015, **44**, 2221.
29 Y. Segawa, H. Omachi and K. Itami, *Org. Lett.*, 2010, **12**, 2262.
30 H. Chen, M. R. Golder, F. Wang, S. K. Doorn, R. Jasti, S. Tretiak and A. K. Swan, *J. Phys. Chem. C*, 2015, **119**, 2879.
31 M. Fujitsuka, S. Tojo, T. Iwamoto, E. Kayahara, S. Yamago and T. Majima, *J. Phys. Chem. Lett.*, 2014, **5**, 2302.
32 S. Tretiak, A. Saxena, R. L. Martin and A. R. Bishop, *Phys. Rev. Lett.*, 2002, **89**, 097402.
33 S. Karabunarliev, E. R. Bittner and M. Baumgarten, *J. Chem. Phys.*, 2001, **114**, 5863.
34 M. J. Frisch, *Gaussian 09*, 2009.
35 T. Yanai, D. P. Tew and N. C. Handy, *Chem. Phys. Lett.*, 2004, **393**, 51.
36 J. P. Perdew, K. Burke and M. Ernzerhof, *Phys. Rev. Lett.*, 1996, **77**, 3865.
37 C. Lee, W. Yang and R. G. Parr, *Phys. Rev. B: Condens. Matter Mater. Phys.*, 1988, **37**, 785.
38 I. H. Nayyar, E. R. Batista, S. Tretiak, A. Saxena, D. L. Smith and R. L. Martin, *J. Phys. Chem. Lett.*, 2011, **2**, 566.
39 I. H. Nayyar, E. R. Batista, S. Tretiak, A. Saxena, D. L. Smith and R. L. Martin, *J. Chem. Theory Comput.*, 2012, **9**, 1144.
40 J.-D. Chai and M. Head-Gordon, *J. Chem. Phys.*, 2008, **128**, 084106.
41 J.-D. Chai and M. Head-Gordon, *Phys. Chem. Chem. Phys.*, 2008, **10**, 6615.
42 O. A. Vydrov and G. E. Scuseria, *J. Chem. Phys.*, 2006, **125**, 234109.
43 J. Heyd, G. E. Scuseria and M. Ernzerhof, *J. Chem. Phys.*, 2003, **118**, 8207.
44 I. H. Nayyar, E. R. Batista, S. Tretiak, A. Saxena, D. L. Smith and R. L. Martin, *J. Polym. Sci., Part B: Polym. Phys.*, 2013, **51**, 935.
45 J. Autschbach and M. Srebro, *Acc. Chem. Res.*, 2014, **47**, 2592.
46 B. Moore, A. Charaf-Eddin, A. Planchat, C. Adamo, J. Autschbach and D. Jacquemin, *J. Chem. Theory Comput.*, 2014, **10**, 4599.
47 A. J. Garza, O. I. Osman, A. M. Asiri and G. E. Scuseria, *J. Phys. Chem. B*, 2015, **119**, 1202.
48 I. Franco and S. Tretiak, *J. Am. Chem. Soc.*, 2004, **126**, 12130.
49 S. Louie, in *Electronic Band Structure and Its Applications*, ed. M. Yussouff, Springer Berlin Heidelberg, London, 1987, vol. 283, p. 93.
50 J. Clark, T. Nelson, S. Tretiak, G. Cirmi and G. Lanzani, *Nat. Phys.*, 2012, **8**, 225.
51 M. Kasha, *Discuss. Faraday Soc.*, 1950, **9**, 14.
52 J. Xia and R. Jasti, *Angew. Chem., Int. Ed.*, 2012, **51**, 2474.
53 A. L. Kitt, Z. Qi, S. Rémi, H. S. Park, A. K. Swan and B. B. Goldberg, *Nano Lett.*, 2013, **13**, 2605.
54 Y. I. Park, C.-Y. Kuo, J. S. Martinez, Y.-S. Park, O. Postupna, A. Zhugayevych, S. Kim, J. Park, S. Tretiak and H.-L. Wang, *ACS Appl. Mater. Interfaces*, 2013, **5**, 4685.
55 D. Hertel, S. Setayesh, H. G. Nothofer, U. Scherf, K. Müllen and H. Bässler, *Adv. Mater.*, 2001, **13**, 65.
56 E. U. Condon, *Phys. Rev.*, 1928, **32**, 858.

